2

BRIEF APPROACH TO MAGNETISM AT THE NANOSCALE

This chapter consist of an introduction to the field of nanomagnetism emphasizing the magnetic interaction between different nanostructures (here ultrathin films) with different magnetic properties. Although old, but not yet fully understood, exchange bias (EB) - one of the most interesting effects in magnetism - is shortly presented.

Contents

2.1 Magnetic interactions between FM and AFM material

2.1.1 Exchange anisotropy

The unidirectional exchange anisotropy (later known as the Exchange Bias (EB) effect) was first discovered by Meiklejohn and Bean as early as 1956 [1, 22] when studying oxidized Co particles. They observed a horizontal shift in the hysteresis loops for the field-cooled system. It was concluded from the beginning that the observed displacement of the hysteresis loop was due to the existence of the native cobalt oxide layer in which the magnetic Co particles are embedded. Thus, the first conclusion was that is an interfacial effect. From that moment on many studies on exchange bias have been performed on thin film systems composed of ferromagnetic (FM) layers in contact with antiferromagnetic (AFM) layers[1].

Figure 2.1 shows the recorded hysteresis loops from the original paper of Meiklejohn and Bean when sample was cooled down to 77 K in zero field (dashed line) and after cooling down (solid line) in a magnetic field of 10 Oe. One can observe that the magnetization curve (dashed line) is centered at zero field at room temperature (the typical behavior of FM materials). The solid line shows the same curve measured after the system is brought to 77 K in a positive magnetic field (known as "field-cooling"). The obvious displacement of the hysteresis loop to negative values can be found even after extremely high fields are applied (70 000 Oe).

For a better view on the EB effect, torque magnetometry has also been used [23]. This can be a very accurate method to measure the magnetocrystalline anisotropy of single crystal ferromagnets. For a small spherical monodomain particle of Co *without* oxide coating, the torque T follows a $\sin(2\theta)$ function (the hysteresis loop recorded after field cooling at 77 K is symmetrically centered):

$$T = -\frac{\partial E}{\partial \theta} = -K_1 \sin 2\theta, \tag{2.1}$$

[1]Throughout this work the nomenclature FM (AFM) was used for either ferromagnetic (antiferromagnetic) or ferromagnet (antiferromagnet)

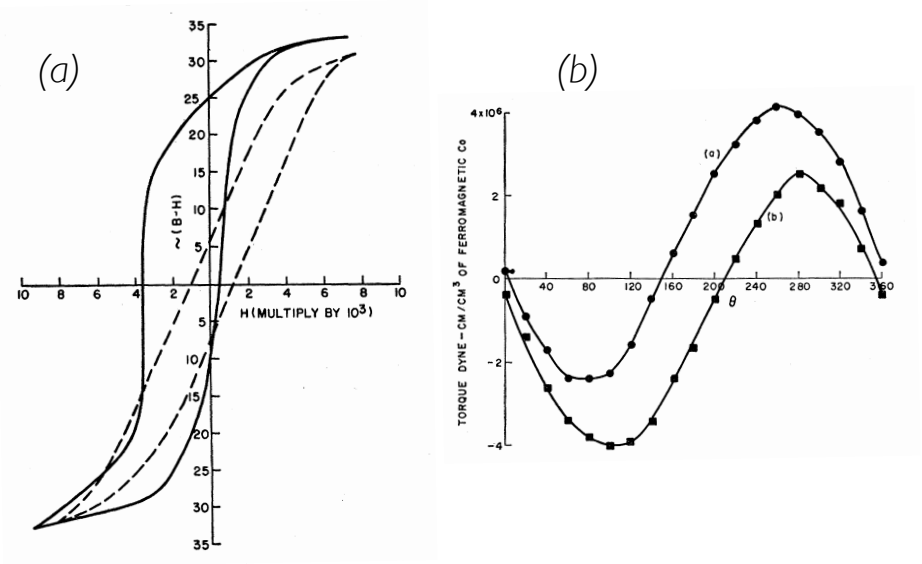

Figure 2.1: Hysteresis loops of oxide-coated Co particles (Co/CoO) system (a) when cooled in zero field (dashed line). The loop is displaced from the axis after the system is cooled in an external magnetic field (solid line). (b) Torque measurements of a field-cooled sample, same as in (a), showing a $\sin(\theta)$ component (the characteristics of unidirectional anisotropy) and rotational hysteresis (separation of the torque curves for the normal and reverse 360° rotations) that can be found also at high magnetic fields [1].

$$E = \int K_1 \sin 2\theta d\theta = K_1 \sin^2 \theta + K_0, \tag{2.2}$$

where K_1 is the magnetocrystalline anisotropy (MCA) constant, K_0 is the integration constant, and θ is the angle between a certain crystallographic direction and the applied magnetic field.

It can be seen that there are two minima of the energy expression at $\theta = 0°$ and $\theta = 180°$, showing that the FM system has two equilibrium states along one axis (nominated c) for these two θ angles.

Considering now the same Co particle but coated with its native oxide and field-cooled to 77 K, the torque curve is a function of $\sin\theta$:

$$T = -\frac{\partial E}{\partial \theta} = -K_u \sin\theta, \tag{2.3}$$

hence,

$$E = \int K_u \sin\theta d\theta = K_u \cos\theta + K_0. \tag{2.4}$$

where K_u represents now the so-called *unidirectional anisotropy* constant.

Last expression for the energy shows that the particles are in equilibrium only for one angle $\theta = 0°$. Taking the system out from this position (namely rotating the sample to an other angle) it will try to return to the starting position. This direction of equilibrium is along the field-cooling direction, and this type of anisotropy is called *unidirectional anisotropy*.

2.1.2 Theoretical models of the exchange anisotropy

Ideal interface model for exchange anisotropy

Figure 2.2 shows the simplest ideal picture of the exchange anisotropy. Both FM and AFM layers are single crystalline and epitaxial; the FM/AFM interface is considered smooth and atomically flat. A particular arrangement of the AFM spins is shown: planes of ferromagnetically coupled spins may exist. The antiparallel coupling happens between these planes, in the direction perpendicular to the surface. The net magnetic moment of the AFM layer is zero. Within this picture, the AFM interfacial plane is fully uncompensated. When an external magnetic field is applied, the spins of the FM layer rotate *coherently*; the magnetic field has no effect on the magnetic structure of the AFM layer.

Unidirectional anisotropy and exchange bias can then be qualitatively understood by assuming an exchange interaction at the FM/AFM interface [1, 23]. When an external magnetic field is applied and $T_N < T < T_C$ (where T_N is the Néel temperature of the AFM, and T_C is the Curie temperature of the FM), the FM spins line up with the field, while the AFM ones remain randomly disordered [Fig. 2.2 (a)]. When cooling to $T < T_N$ in the presence of an external field, due to interfacial interaction, the AFM spins close to interface align parallel to the FM ones (assuming a ferromagnetic interaction at the interface). The next spin plane in the AFM follows the antiferromagnetic order and will be oriented anti-parallel to the previous one. Hence, a zero net magnetization is produced in the AFM. When the field is reversed, the FM spins start to rotate, but, for sufficiently large AFM anisotropy, the AFM spins remain unchanged as shown in Fig. 2.2 (b).

Therefore, the interfacial interaction between the FM and AFM spins at the interface tries to align the ferromagnetic spins parallel with the topmost an-

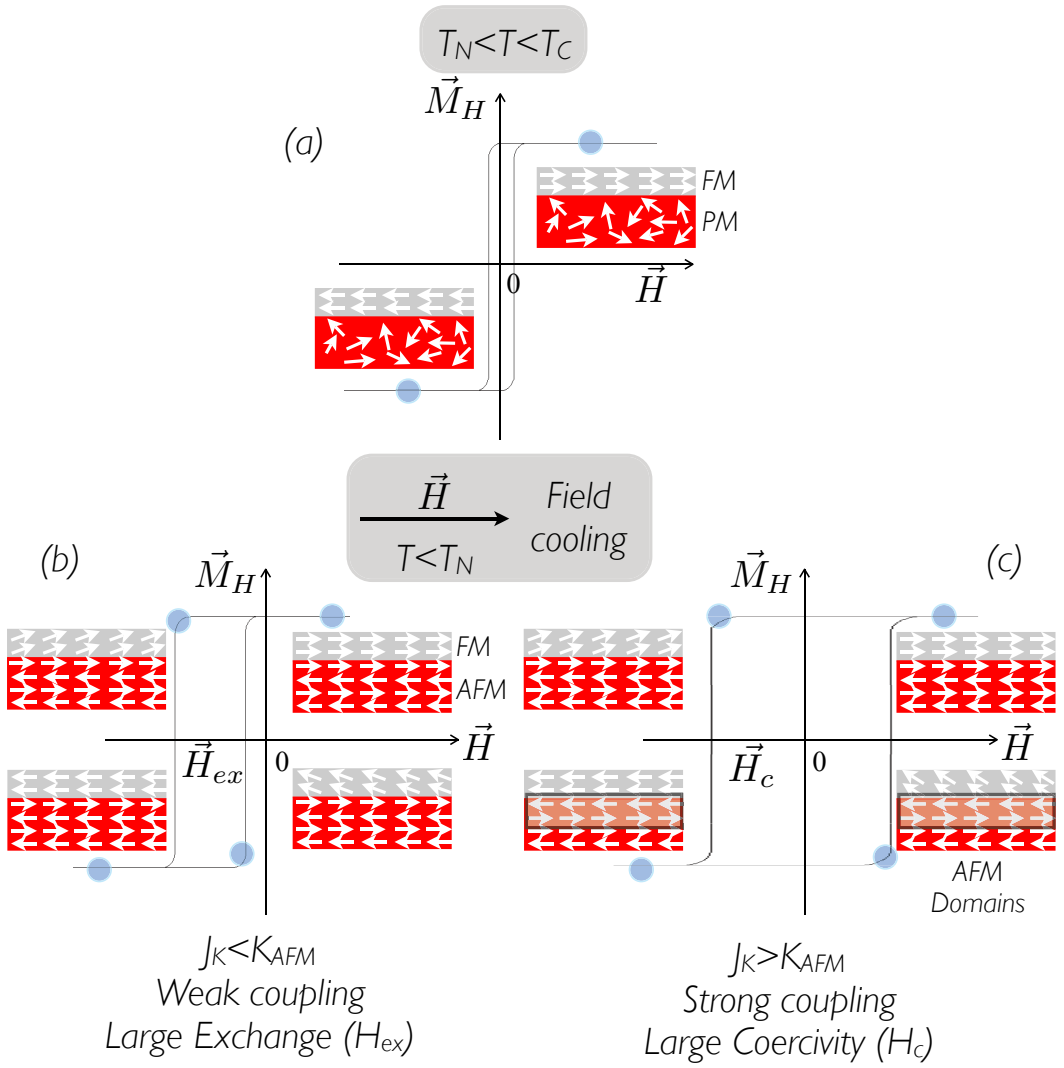

Figure 2.2: Schematic representation of a FM/AFM interface and the spin configuration when $T>T_N$ (a). After field cooling (b, c), depending on different strengths of interfacial couplings, two configurations are evident. The spin configurations are not necessarily in accordance with the real spin rotation of the FM and AFM.

tiferromagnetic spins. In other words, the AFM spins at the interface exert a microscopic torque on the FM spins, to keep them in their original position (ferromagnetically aligned at the interface). Therefore, the FM spins have one single stable configuration: the anisotropy is unidirectional. Thus, the magnetic field needed to reverse the FM layer completely will be larger if it is in contact with an AFM substrate, because an extra field is necessary to overcome the microscopic torque. However, once the field is rotated back to its original direction,

the FM spins will start to rotate at a smaller field, due to the interaction with the AFM spins (which now exert a torque in the same direction as the field). The material behaves as if there was an extra (internal) biasing field, therefore the FM hysteresis loop is shifted [Fig. 2.2 (b)] along the field axis. This was therefore termed *exchange bias* (EB) [1, 23, 24, 25].

The phenomenological formula of the exchange field is:

$$H_{EB} = \frac{\Delta\sigma}{\mu_0 M_{FM} t_{FM}} = \frac{J_K \mathbf{S}_{FM} \mathbf{S}_{AFM}}{a^2 \mu_0 M_{FM} t_{FM}}, \tag{2.5}$$

where $\Delta\sigma$ is the interfacial energy density of the FM/AFM system, J_K is the exchange parameter, $\mathbf{S}_{FM}$ and $\mathbf{S}_{AFM}$ are the spins of the atoms at the interface (in the FM and the AFM layer, respectively), a is the cubic lattice parameter, M_{FM} and t_{FM} are the magnetization and the thickness of the FM layer, respectively. However, this formula predicts exchange fields that are two or three orders of magnitude larger than those observed. With reasonable parameters, the value obtained for $\Delta\sigma$ is of about 10 erg/cm^2, whereas typical experimental values are $\Delta\sigma \approx 0.1$ erg/cm^2. Within this simple picture, the exchange field (*i.e.*, the shift of the hysteresis loop) is qualitatively understood as related to the interaction with the AFM uncompensated spin planes. Although this simple phenomenological model gives an intuitive picture, there is little quantitative understanding of this phenomenon. Moreover, the role of the many different parameters involved in exchange bias, such as anisotropy, roughness, spin configuration or magnetic domains, is far from being understood. Finally, a clear understanding of the exchange bias at the microscopic level is still missing. Different phenomena (interfacial contamination, roughness, crystallinity) have been invoked to account, beside the wide range of reported effects, for the above mentioned reduction of the interfacial coupling strength. The most important models of the exchange bias will be shortly reviewed in the following.

Kouvel, Meiklejohn and Bean's model

The earliest model of the exchange anisotropy was proposed by Kouvel [7, 8, 26] in studies of exchange anisotropy in disordered alloys and Meiklejohn and Bean [1, 23] for exchange anisotropy in oxidised particles and thin films, as previously presented. Although the systems were quite different, similar pictures of the mechanism behind the unidirectional anisotropy were developed.

Starting from the ideal model, it was deduced that the magnetic behavior of these systems depends on the ratio of the interfacial exchange anisotropy constant J_K (exchange energy per surface unit) and the AFM magnetocrystalline anisotropy constant K_{AFM} (magnetocrystalline energy per volume). Three regimes of the magnetic behaviour were distinguished:

- **Weak interfacial coupling ($J_K << K_{AFM}$):** In this case, the FM layer follows the external applied field. The "memory effect" of exchange bias is preserved, due to the unidirectional anisotropy induced by the AFM orientation. In this limit, unidirectional anisotropy but no rotational hysteresis are observed [Fig. 2.2 (b)].
- **Comparable anisotropy energies ($J_K \approx K_{AFM}$):** The magnetization of the AFM starts from its original easy axis direction, but more slowly than the FM component. At a certain (critical) angle, the AFM axis changes abruptly (rotates by 180° with respect to the initial configuration). Due to the discontinuous reversal of the AFM magnetic lattice, the system will exhibit rotational hysteresis but no unidirectional anisotropy (the "memory effect", *i.e* the AFM single domain configuration created by the field cooling procedure, is removed by the reversal of the AFM lattice).
- **Strong interfacial coupling ($J_K >> K_{AFM}$):** The magnetization axis of the AFM component (still retaining the antiparallel configuration) follows closely the magnetization of the FM component, which is rotated in a large external magnetic field (energy is dissipated in rotating the AFM, creating magnetic domains). In this limit, neither rotational hysteresis nor a unidirectional anisotropy are observed. Large coercivities will be measured for the FM component [Fig. 2.2 (c)].

The temperature dependence of the magnetic behaviour of the system is reflected by the variation of the ratio J_K/K_{AFM} with temperature: J_K is temperature independent, but K_{AFM} does vary with the temperature. When the temperature is close to the Néel temperature of the AFM (*i.e*, K_{AFM} is very small), the model predicts no unidirectional anisotropy, nor rotational hysteresis. As the temperature decreases, K_{AFM} starts to become more and more important, and then, depending on the J_K value, the model predicts an increase in the exchange field.

This model is applicable for any FM/AFM interface and offers a qualitative explanation of the effect (presence or absence of exchange field and rota-

tional hysteresis).

Mauri's model

In order to explain the discrepancies between the exchange field values predicted by a simple theory like the ideal interface model (Eq. 2.5) and experimentally measured values, Mauri [12] proposed a mechanism to effectively lower the interface energy cost in reversing the FM layer without removing the conditions of a strong interfacial FM/AFM coupling: Formation of planar domain walls at the interface with the reversal of the FM magnetization orientation.

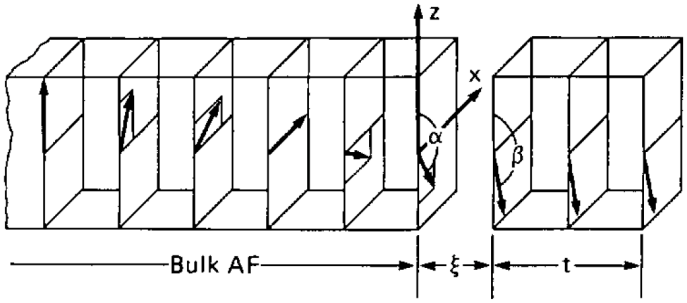

Figure 2.3: Mauri's model of the FM/AFM interface [12]. Here the AFM spins are not fix anymore; their rotation is creating a domain wall parallel to the interface. The arrows in the AFM are shown only for one magnetic sublattice.

The domain wall could be either in the FM or AFM layer, depending on which has the smallest energy. Mauri examined the case where the domain wall is on the AFM side of the interface. Thus, the exchange field will be:

$$H_{ex} = \frac{2\sqrt{A_{AFM}K_{AFM}}}{\mu_0 M_{FM} t_{FM}}, \tag{2.6}$$

where A_{AFM} and t_{FM} are the exchange stiffness of the antiferromagnetic layer and the thickness of the ferromagnetic layer, respectively.

By spreading the exchange energy ($\sim \pi\sqrt{A_{AFM}K_{AFM}}$) over a domain wall width instead of a single atomic interface with lattice constant a, the interfacial exchange energy is reduced by a factor of $\pi\sqrt{A_{AFM}K_{AFM}}/a \sim 100$, which is expected to provide the correct reduction to be consistent with the observed values.

The premises of the model:

- An AFM domain wall can form at the interface;
- The AFM layer is infinitely thick (no restriction of the AFM domain wall formation due to thickness);
- Coherent rotation of the FM spins.

The Hamiltonian used for this model takes into account the AFM domain wall energy, the interfacial exchange energy, the FM anisotropy energy and a magnetostatic energy term [12]. Two limiting cases are obtained:

- **weak interfacial coupling** ($J_K << \sqrt{A_{AFM}K_{AFM}}$):

$$H_{eb} = -\frac{J_K}{\mu_0 M_{FM} t_{FM}}, \tag{2.7}$$

- **strong interfacial coupling** ($J_K >> \sqrt{A_{AFM}K_{AFM}}$):

$$H_{eb} = -2\frac{\sqrt{A_{AFM}K_{AFM}}}{\mu_0 M_{FM} t_{FM}}. \tag{2.8}$$

where J_K is the interfacial exchange coupling parameter, and θ_{FM} and M_{FM} are the thickness and saturation magnetization of the FM layer, respectively.

The temperature dependence of the exchange bias field is given, like in the previous model, by the temperature dependence of K_{AFM}.

This simple one-dimensional model does not examine characteristics such as thin AFM films, compensated interfaces, polycrystallinity, interfacial roughness.

Malozemoff's model

Mauri's model proposes a perfect, atomically uncompensated interface exchange. In order to approach reality, Malozemoff proposed a model of random fields [9, 10] that takes into account interfacial roughness down to the atomic scale, and does not rely on the conditions of an ideal interface. In this model, the interfacial AFM moment imbalance is due to roughness and structural defects.

One might expect that the interface energy decreases to zero with the increase of the defect density. On the contrary, Malozemoff proposed that these interfacial inhomogeneities create localised sites with unidirectional interface

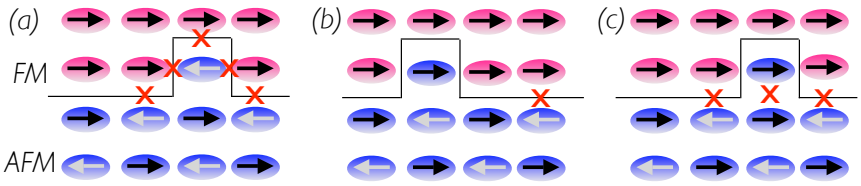

Figure 2.4: Malozemoff's model of the interface [9]. Schematic side view of a possible atomic moment configuration for a non-planar FM/AFM interface. The solid line is the separation between FM (top) and AFM (bottom) layers. The bump (framed by the continuos line) should be visualized on a two-dimensional interface. Configuration (c) is just a lower energy state of (a). The shifted bump (b) is energetically equivalent to flipping the ferromagnetic spins in (a).

energy. For an interface with atomic-scale roughness, the local unidirectional interface energy is also random,

$$\sigma = \pm z \frac{J_K}{a^2} \tag{2.9}$$

where J_K is the interfacial exchange parameter, a is the cubic lattice parameter, and z is of the number of order unity. Despite the randomness of σ, the random-field theory argues that statistically a net averaged non-zero interfacial energy will exist, particularly when the average is taken over a small number of sites. Statistically, $\langle\sigma\rangle \approx \sigma/\sqrt{N}$, where $N = L^2/a^2$ is the number of sites projected onto the interface plane. Assuming a single-domain FM film, the AFM will divide into domain-like regions to minimise the net random unidirectional anisotropy. Unlike Mauri's model, the AFM domain walls are now normal to the interface. The AFM domain structure (around defects) is occurring when the FM/AFM interface is cooled through T_N. It is favorable that the domain size L expands to lower the energy; however, it will be the in-plane uniaxial anisotropy K_{AFM} in the AFM film, which will limit its size. The domain wall width will be confined by the anisotropy to $\pi\sqrt{A_{AFM}/K_{AFM}}$ $(< L)$ and will create an additional surface energy term of the domain wall ($4\sqrt{A_{AFM}/K_{AFM}}$, surface tension in sphere). The exchange and anisotropy terms will compensate when $L \approx \pi\sqrt{A_{AFM}/K_{AFM}}$. Thus, the average interfacial energy density will be:

$$\Delta\sigma = \frac{4zJ_K}{\pi aL} \tag{2.10}$$

and the exchange field

$$H_{ex} = \frac{\Delta\sigma}{2\mu_0 M_{FM} t_{FM}} = \frac{2z\sqrt{A_{AFM}/K_{AFM}}}{\pi^2 \mu_0 M_{FM} t_{FM}}. \tag{2.11}$$

This equation is very similar to the strong interfacial case (Eq. 2.8) of Mauri's model. Quantitatively, the random field model also accounts for the 10^{-2} reduction of the exchange field with respect to the ideal interface model.

Despite being more realistic, this model does not include any discussion concerning polycrystalline samples.

Koon's model

Following results of micromagnetic numerical calculations, Koon proposed the existence and stability of an unidirectional anisotropy in thin films with a fully compensated FM/AFM interface by a stabilisation of the interface exchange coupling with a perpendicular orientation between the spin of the FM and AFM layers [11]. The perpendicular orientation between the FM and AFM spin axes with a compensated AFM interface is purely a result of the minimisation of the interface exchange energy, and not a bulk effect.

This model examines a very specific system. To observe the unidirectional anisotropy due to perpendicular coupling, this model specifies the AFM structure, the AFM crystalline orientation, and the relative orientation between the AFM and FM layer. The results are suggestive, but difficult to apply directly to other systems: Koon's model uses a single crystal body centred tetragonal *bct* AFM either with fully uncompensated {100} or fully compensated {110} crystallographic planes. No anisotropy was considered for the FM layer, and a uniaxial one for the AFM layer. For both cases mentioned above, Koon calculated the interfacial energy density with respect to the angle θ between the FM and AFM spins. While the fully uncompensated interface yields a minimum corresponding to collinear coupling ($\theta = 0°$), the fully compensated one surprisingly results in $\theta = 90°$. Koon also suggested that the roughness would reduce the frustration and biasing as compared to the compensated case. It also seems that when introducing roughness into his model, the coupling tends to a transition into a collinear one [27].

However, this approach may be more relevant for smooth single crystals than for polycrystalline films. A similar model was developed for metallic mul-

tilayers (FM/NM/FM) by Demokritov [28], trying to implement the existence of such a coupling for a multitude of systems. Here it has to be stressed that to obtain exchange bias form Koon's model, in addition Mauri's model must be used.

Takano's model

This model was developed by Takano *et al.* [29] to explain the results of FeNi/CoO interfaces. The model is based on the influence of the exchange bias field (H_{ex}) to the interfacial density of uncompensated spins. It can be applied to FM/CoO (111) samples in the case of terraces at the interfaces. For polycrystalline samples, the size of terraces and the dimensions of the crystallites are playing an important role. The exchange field is finally deduced as:

$$H_{ex} = \frac{[U_{tot}^{FC}(-S_{FM}) - U_{tot}^{FC}(+S_{FM})]}{2\mu_0 M_{FM}\theta_{FM}} \cdot \frac{1}{area} \tag{2.12}$$

where U_{tot} is the total interfacial energy calculated from all the single crystallite interfacial energies, and FC stands for field cooled below the Néel temperature of the AFM layer. $-S_{FM}$ and $+S_{FM}$ are the two orientations of the FM layer (parallel and antiparallel), M_{FM} is the magnetization of the FM layer and θ_{FM} its thickness. Roughness can also be introduced.

The model predicts an inverse relationship between H_{ex} and the grain diameter measured experimentally.

Domain state model

The domain state model is a microscopic model based on a magnetic disorder introduced by a magnetic dilution not only at the interface but also in the bulk of the AFM layer. The basis of the model consists in an AFM layer having the properties of a diluted Ising antiferromagnet in an applied (external) field (DAFF) which has a phase diagram like the one presented in Fig. 2.5 (right). In zero field, the system undergoes a magnetic phase transition from a paramagnetic state to a long-range-ordered antiferromagnetic phase at T_N which in this case is dilution-dependent. When the field is increased at low temperature, the diluted AFM exhibits a domain state (DS) phase having a spin-glass behavior. The formation of the DS phase is due to a statistical imbalance of the amount

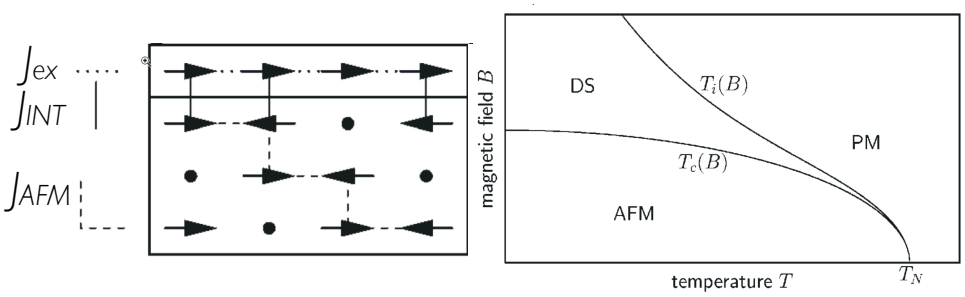

Figure 2.5: Domain state model of the interface. The sketch presents one ferromagnetic layer and three diluted antiferromagnetic layers. The respective coupling is noted on in the figure. The graph shows the phase diagram of a diluted antiferromagnet [30].

of impurities between the two AFM sublattices, leading to a net magnetization which couples to the external magnetic field. A spin flip of the magnetization, *i.e.* creation of a domain, lowers the energy of the system. The energy needed for the formation of a domain wall can be minimized if the domain wall passes through nonmagnetic defects.

The FM is described by a classical Heisenberg model containing the nearest-neighbor exchange constant J_k. The AFM can be described, as already mentioned before, as a magnetically diluted Ising system. The easy axis of the AFM is parallel to the FM one. The Hamiltonian of the system using d_x and d_z for the anisotropy constants can be written as [30]:

$$\begin{aligned} H &= -J_k \sum_{\langle i,j\rangle \in FM} \mathbf{S_i S_j} - \sum_{i \in FM} (d_z S_{iz}^2 + d_x S_{ix}^2 + \mu_0 m \mathbf{H S}_i) \\ &\quad -J_{AFM} \sum_{\langle i,j\rangle \in AFM} \epsilon_i \epsilon_j \sigma_i \sigma_j - \sum_{i \in AFM} \mu_0 m H_z \epsilon_i \sigma_i \\ &\quad -J_{INT} \sum_{\langle i \in AFM, j \in FM\rangle} \epsilon_i \sigma_i S_{jz}, \end{aligned} \tag{2.13}$$

where $\mathbf{H}$ is the magnetic field applied, $\epsilon_{i,j}$ are parameters used to describe fractions of sites carrying ($\epsilon_i = 0$) or not carrying ($\epsilon_i = 1$) a magnetic moment m, the $\mathbf{S}_i$ and σ_i represent the classical dimensionless spin vectors for the FM and AFM, respectively. The first line in Eq. 2.13 represents the energy contribution of the FM layer, the second line corresponds to the AFM layer, and the third includes the exchange coupling between the FM and the diluted AFM layer.

It was experimentally shown that the EB depends of the bulk properties of the diluted AFM, but also on the concentration of the dilution impurities. It

appears that at zero dilution, the DS gives vanishing exchange bias. The exchange bias is missing at low dilutions because the domains in the AFM cannot be formed as they would cost too much energy to break the AFM bonds.

Overall, it is believed that strong support for the DS model is given by experimental observations where nonmagnetic impurities are added to the AF layer in a systematic and controlled way [31, 32, 33, 34]. Also, it appears that a good agreement is observed with the experiments shown in Ref. [35], where the dependence of the EB on the AFM thickness and temperature for IrMn/Co is presented.

Other models

Other models that have been put forth include the formation of domains in the FM layer [36, 37], field effects on the AFM layer [38], grain size distribution [39, 40], and induced thermoremanent magnetization in the AFM layer [41].

These models have attained different degrees of agreement with existing experimental results. However, their general feature, as soon as they try to address the exchange coupling in a quantitative manner, is their limited validity to only one system or a particular type of interface, while they are not valid for other systems. Only few parameters can be varied and described using one model. Most models assume the interface plane to be homogeneous (*i.e.* they are uni- or two-dimensional), the AFM and FM anisotropy axis to be collinear, and/or the AFM moment at the interface to be uncompensated.

2.2 CoO as an antiferromagnetic system

2.2.1 General overview on transition-metal oxides

From all transition-metal (TM) elements (Sc, Ti, V, Cr, Mn, Fe, Co, Ni, and Cu) only two, namely Sc and Cr, do not form stable monoxides, *i.e.* ScO and CrO. The physical properties of the oxides are very sensitive to oxygen stoichiometry. Also their electric conductivity properties may drastically vary, depending on the TM element involved. As an example, TiO can be a metallic conductor and a superconductor, VO is a semimetal, whereas MnO, FeO, CoO, NiO, CuO are weak semiconductors with an antiferromagnetic ordering below their Néel

Oxide	Electronic Configuration		Insulating Gap	Néel Temperature	Lattice Constant
	O^{2-}	TM^{2+}	(eV)	(K)	(nm)
MnO	[He] $2s^2 2p^6$	[Ar] $3d^5$	3.6–4.2	118	0.444
CoO	[He] $2s^2 2p^6$	[Ar] $3d^7$	2.5–6	289	0.426
NiO	[He] $2s^2 2p^6$	[Ar] $3d^8$	3.1–4.3	523	0.417

Table 2.1: General electronic and structural properties of main TM - oxides.

temperature. Co oxide can also be found in another stable state as a Co_3O_4; in this work we refer only to the CoO (1×1) – Co monoxide.

Table 2.1 presents, from left to right, some of the most important electronic and structural properties of the main transition-metal oxides: electronic configuration, insulating gap, bulk Néel temperature and bulk lattice constant.

2.2.2 Structural, electronic and magnetic properties

The transition metal oxide CoO, same as its equivalents MnO, NiO, forms an ionic antiferromagnetic rock-salt crystal structure. Figure 2.6 shows the phase diagram for the Co–CoO–Co_3O_4 system formation; proper oxygen pressure and temperature can lead to CoO (monoxide) formation [42, 43].

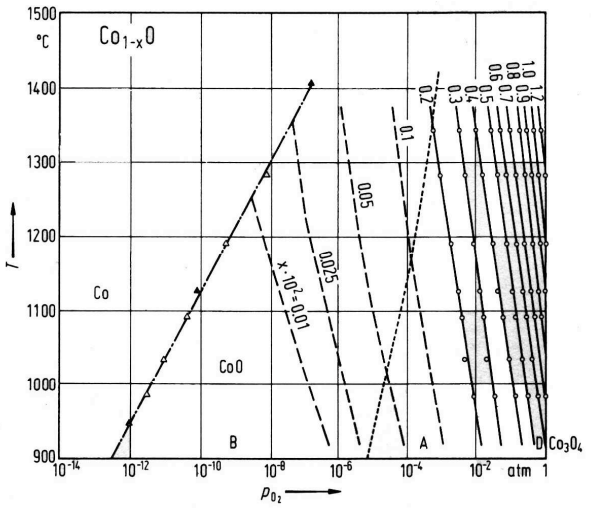

Figure 2.6: The phase diagram for Co–CoO–Co_3O_4 oxide formation [42]. Note that higher oxygen pressure leads to the formation of Co_3O_4 type of oxide with spinel–like structure [44].

In the case of CoO, two transition-metal electrons are fully filling the O $2p$ shell, thus resulting in O^{2-} ions ([He] $2s^2 2p^6$ configuration) and TM^{2+} ions

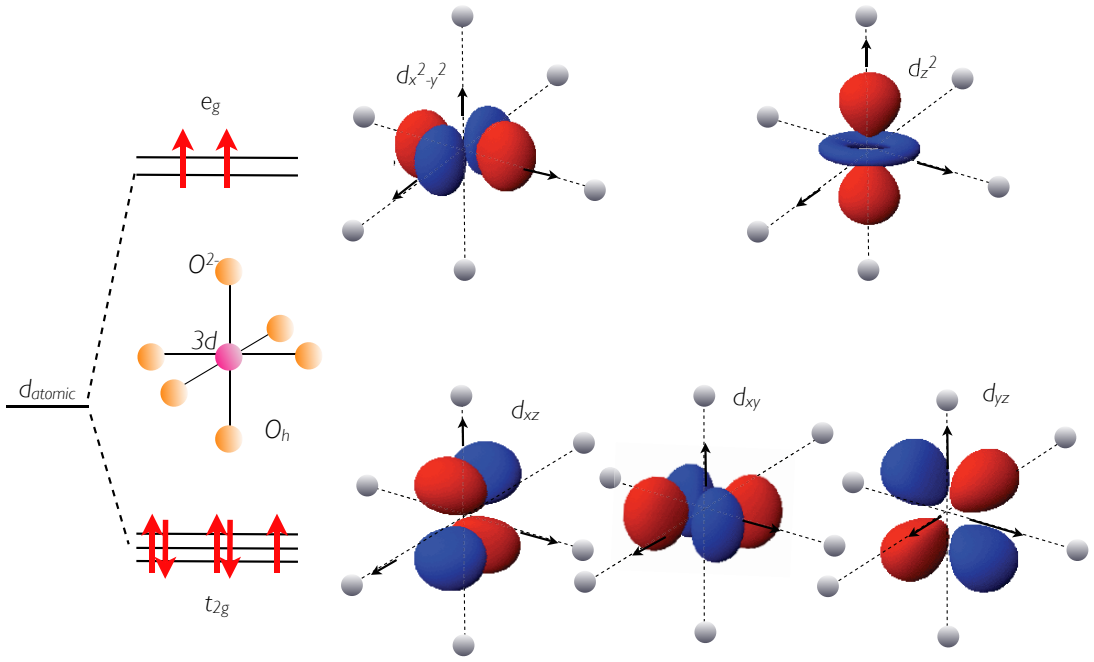

Figure 2.7: Crystal field splitting of the atomic levels in the case of a Co atom surrounded by six oxygen atoms in a O_h symmetry [45].

([Ar] $3d^7$ configuration) [45]. The chemical bond is not purely ionic but also contains covalent contributions. Without any hybridization between the anion and cation orbitals, the dipole allowed O $1s$ – O $2p$ transition is impossible due to the closed O $2p$ shell of the O^{2-} ion. Nevertheless, the X-ray absorption spectra show a high intensity near the O $1s$ threshold, which can be attributed to the reduction of the number of filled states with O $2p$ character due to the O $2p$/TM $3d$ hybridization [42].

The CoO $3d$ states can not be easily described using the pure band structure picture; in this case the d electrons behave similarly to those of free atoms or ions, and the degeneracy of the $3d$ state concerning the m_l quantum number is partially lifted. In the most simple picture, the Co ion is surrounded by six O^{2-} ions in an octahedral symmetry [45]. The $3d$ states, completely degenerated in a spherical symmetry of a free atom, in this octahedral conformation are energetically split and a crystal-field multiplet occurs. The crystal field splitting is usually presented in a "one-electron picture" (Fig. 2.7), where a single d electron is in the middle of an O_h environment of negative point charges (the oxygen atoms). Whereas the e_g orbitals are directed towards the oxygen ions, located on the axes as shown in the figure, the lobes of the t_{2g} orbitals are situ-

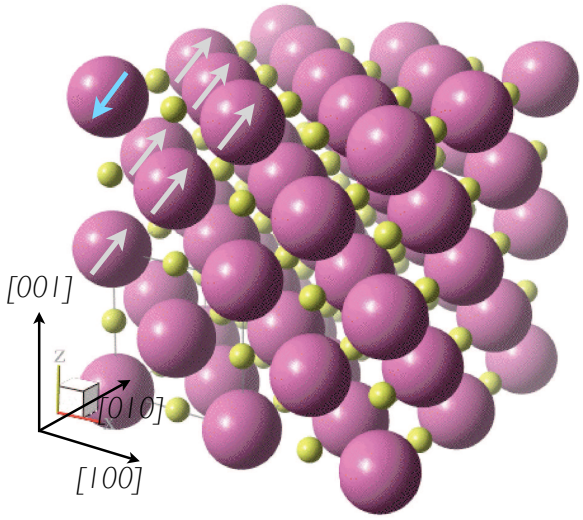

Figure 2.8: Simplified model of the type-II collinear AFM order in bulk CoO systems. The spins are aligned in {111} planes, each neighbor plane showing an antiferromagnetic orientation of their spins [45, 46]. The representation of the size of the atoms is exaggerated.

ated in between the oxygen ions. Therefore, a $3d$ electron in the e_g orbital "feels" a Coulomb potential different from the one of the t_{2g} orbitals. Thus the e_g and t_{2g} levels are separated by Δ_{CF} (in the spectroscopic notation Δ_{CF} = 10Dq) [45].

Above the Néel temperature, the crystal structure of the oxide is cubic (*fcc*, known as the rock-salt structure) and it is magnetically disordered (paramagnetic state). The lattice constant of CoO is a = 4.26 Å (a = 4.177 Å for NiO) [46]. Below the Néel temperature the system exhibit spontaneous AFM ordering that is known to be type-II antiferromagnet. In the CoO (*fcc*) sublattice along the [100] direction, one can find the Co spins (separated by the oxygen atoms) being coupled antiferromagnetically [47] so that the {111} planes are having the spins ordered ferromagnetically; adjacent {111} planes show an antiferromagnetic order with respect to the latter.

In the case of bulk CoO, a large amount of experimental and theoretical work has been done in order to explain in detail the AFM order. For this system, accompanying the paramagnetic–antiferromagnetic transition, there is also a crystallographic one, during which the system passes from a cubic lattice structure (a = 4.26 Å) to a monoclinic one (a = 5.18 Å, b = 3.017 Å, c = 3.18 Å [48]), observed for the first time by Tombs *et al.* [49]. The magnitude of this distortion increases linearly with decreasing temperature [46].

Reviewing the theory of antiferromagnetism by Nagamiya, Kubo and Yoshida [50], two mechanisms for the deformation below the Néel temperature have been found: one is the magnetostriction that arises from large anisotropy

energies and depends on the orientation of the magnetic moments; another one is the ”exchange-striction”, which comes from the dependence of the exchange energies on interatomic distances [51].

Van Laar *et al.* [52] have shown by means of powder neutron diffraction that the magnetic directions are tilted out of the {111} plane by an 8° angle. They were also proposing a multiaxis spin structure with a tetragonal symmetry [53]. By neutron diffraction experiments it is difficult to determine the real structure of bulk CoO (even for single crystals) because the Bragg peaks have the same intensities for both the multiaxis model and the collinear structure with multidomain configuration [54]. X-ray diffraction data and torque measurements failed to verify the multiaxis model [55, 56, 57].

Therefore, Richtin and Averbach [47] presented an AFM structure of CoO with the spins parallel aligned in the {111} planes but having a tilt angle of 7°. They argued that the spin axis does not change its direction with temperature for measurements between 4.2 K and 272 K. Fine *et al.* [58] were trying to explain the CoO AFM behavior using the temperature dependence of Young's modulus.

The recent work of Tomiyasu *et al.* [59] is complicating the problem even more. Using neutron and X-ray diffraction techniques they have proven that, accompanying the tetragonal distortion already known, there is a trigonal one, the combination of these two leading to a combination of type-I and type-II antiferromagnetic order. Finally they proposed a monoclinic structure for CoO.

The structure of epitaxially deposited CoO on Ag(001) was studied by means of Scanning Tunneling Microscopy (STM) [60, 44] and Low Energy Electron Diffraction (LEED) for a coverage between 1 to 5 ML CoO [61] showing that even though the lattice mismatch is 4.3% between the CoO and the Ag(001) substrate, the oxide is growing in an ordered mode, following the substrate crystallographic structure. A vertical expansion of the film structure was also detected. Another approach, from the electronic and magnetic point of view can be found in a publication by Csiszar *et al.* [5]. They studied CoO films deposited on different substrates that can induce different strain in the oxide film. For example they compared the CoO deposited on Ag(001) with CoO sandwiched between MnO finding the same type of structural expansion predicted by Wang *et al.* [61] for CoO/Ag(001) what was later called “milk-box” expansion, and a reduction of the perpendicular lattice parameter for the MnO/CoO/MnO/Ag(001) system, called “pizza-box” expansion. Experiments were performed on 90 Å epi-

taxially deposited single-crystalline CoO. These two types of strain have a major influence on the electronic and magnetic properties of CoO. They concluded that the spin axis in the first case is in the film plane, whereas for the second case the axis shows a large out-of-plane component.

Exchange bias–related work was carried out by Radu *et al.* using CoO as the antiferromagnetic layer in the system [6, 62, 63]. The sputter–deposited Co/CoO and Fe/CoO bilayers were used to study the dependence of EB and coercive fields on the thickness of the ferromagnet and to study the asymmetry of the hysteresis loops and the temperature dependence of the critical fields [48, 50]. Soft X-ray resonant magnetic scattering (XRMS) was used to get complementary information with respect to Polarized Neutron Reflectometry (PNR) [62]. Through its element specific property it was studied particularly the induced ferromagnetic components in the AFM CoO layer.